JBC RESEARCH ARTICLE

Identification of the riboflavin cofactor-binding site in the *Vibrio cholerae* ion-pumping NQR complex: A novel structural motif in redox enzymes

Received for publication, April 27, 2022, and in revised form, June 16, 2022 Published, Papers in Press, June 23, 2022,
https://doi.org/10.1016/j.jbc.2022.102182

Karina Tuz[1], Ming Yuan[1], Yuyao Hu[1], Tien T. T. Do[2], Soohaeng Yoo Willow[2], Joseph A. DePaolo-Boisvert[2], James R. Fuller[3], David D. L. Minh[2], and Oscar Juárez[1,*]

From the [1]Department of Biological Sciences, and [2]Department of Chemistry, Illinois Institute of Technology, Chicago, Illinois, USA; [3]Department of Biochemistry and Molecular Biology, University of Chicago, Chicago, Illinois, USA

Edited by Ruma Banerjee

The ion-pumping NQR complex is an essential respiratory enzyme in the physiology of many pathogenic bacteria. This enzyme transfers electrons from NADH to ubiquinone through several cofactors, including riboflavin (vitamin B2). NQR is the only enzyme reported that is able to use riboflavin as a cofactor. Moreover, the riboflavin molecule is found as a stable neutral semiquinone radical. The otherwise highly reactive unpaired electron is stabilized *via* an unknown mechanism. Crystallographic data suggested that riboflavin might be found in a superficially located site in the interface of NQR subunits B and E. However, this location is highly problematic, as the site does not have the expected physiochemical properties. In this work, we have located the riboflavin-binding site in an amphipathic pocket in subunit B, previously proposed to be the entry site of sodium. Here, we show that this site contains absolutely conserved residues, including N200, N203, and D346. Mutations of these residues decrease enzymatic activity and specifically block the ability of NQR to bind riboflavin. Docking analysis and molecular dynamics simulations indicate that these residues participate directly in riboflavin binding, establishing hydrogen bonds that stabilize the cofactor in the site. We conclude that riboflavin is likely bound in the proposed pocket, which is consistent with enzymatic characterizations, thermodynamic studies, and distance between cofactors.

The ion-pumping respiratory complex NQR[1] is the first enzyme in the electron transport chain of *Vibrio cholerae* and many other human pathogenic bacteria (1–4). NQR catalyzes the electron transfer from NADH to ubiquinone (UQ) (1, 5, 6), similar to the activity of mitochondrial complex I. In *V. cholerae*, NQR activity is coupled to the pumping of sodium ions, which generates a transmembrane electrochemical gradient (7). The ion gradient is used to support many essential processes, such as pH regulation, drug efflux, nutrient transport, flagellum rotation, (2, 3, 8–10). NQR also plays an important role in the production of virulence factors such as the cholera toxin and the toxin coregulated pillus (11, 12), and the inactivation of the nqr operon abolishes *V. cholerae* pathogenicity (13). Our group has recently shown that NQR also fulfills essential roles in the physiology of the obligate intracellular pathogen *Chlamydia trachomatis* (14), responsible for one of the most common sexually transmitted infections in the world (15, 16), and *Pseudomonas aeruginosa* (17), one of the leading causes of multidrug-resistant and hospital-acquired infections (17–20). Because of its critical role in microbial physiology and its absence in human cells, NQR has been proposed as a potential drug target (14, 21).

NQR is composed of six subunits (A–F) and five confirmed redox cofactors (Fig. 1*A*): FAD, two covalently attached FMN molecules, a 2Fe-2S center, and riboflavin (1, 8, 22, 23). Subunit A is cytosolic with a putative role in complex assembly (24, 25). Subunits B and C each contain a covalently bound FMN (1, 26, 27), which is attached by the only known flavin transferase, ApbE (28, 29). Subunits D and E contain six transmembrane subunits and seem to carry a nonheme iron center (22). While this iron center has been proposed to have a role in electron transfer (5, 22), it has not been confirmed experimentally. Subunit F has a large hydrophilic domain facing the cytosol that carries FAD and a 2Fe-2S center and a transmembrane segment that anchors it to the cell membrane (13, 22). Kinetic characterizations, along with stopped flow data, allowed us to propose a reaction scheme that explains the catalytic mechanism of the complex (27, 30). Briefly, NADH oxidation occurs in the hydrophilic domain of subunit F, where the noncovalently bound cofactor FAD accepts two electrons from NADH, one of which subsequently accepted by the 2Fe-2S center. The electron could be transferred to the nonheme Fe center in subunits D and E (5, 22) and then to the covalently bound FMN in subunit C (FMN_C), which is the redox step associated with sodium capture (31). The electrons are transferred from FMN_C to FMN in subunit B (FMN_B) (26, 27, 31) and finally to riboflavin (1, 26), which is the step associated with sodium translocation (31). Subsequently, the electrons are delivered to UQ, the second substrate of the redox reaction (27).

NQR's riboflavin-binding site is of particular interest in flavin biochemistry, biological redox chemistry, and

* For correspondence: Oscar Juárez, ojuarez@iit.edu.

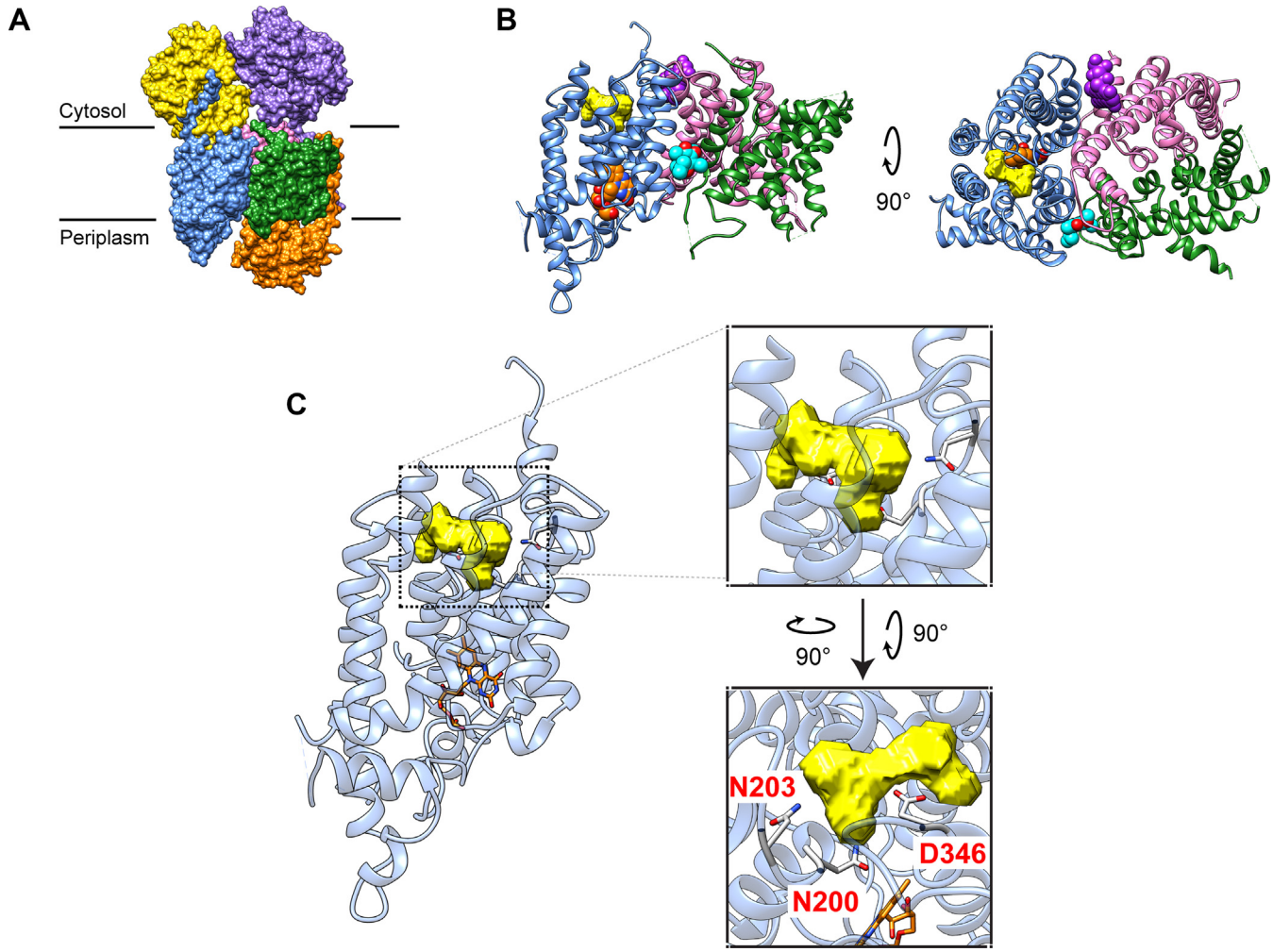

Figure 1. Location of the crystallographic riboflavin and the proposed riboflavin-binding pocket. *A*, tridimensional model of NQR with subunits A (*yellow*), B (*blue*), C (*orange*), D (*green*), E (*pink*), and F (*violet*). *B*, transmembrane subunits B, D, and E showing the location of FMN_B (*orange*), ubiquinone (*cyan*), crystallographic riboflavin (*purple*), and the empty pocket assigned as the riboflavin-binding site (*yellow*). *Left panel*: The orientation of the subunits is the same as shown in (*A*). *Right panel*: the subunits are rotated 90° along the *horizontal axis*, offering a *top* view of the structure. *C*, empty pocket (*yellow*) proposed as the riboflavin-binding site in subunit B (*blue* semitransparent). Residues N200, N203, and D346 are shown in the figure in the pocket. *Top right panel*: Zoom into the site. *Bottom right*: *Horizontal* (90°) and *vertical* (90°) rotation of the subunit to illustrate the position of the residues in the site.

structure-based drug design. NQR has an evolutionary history divergent from those of other respiratory enzymes and ion pump families, and it has evolved unique structural motifs, reaction mechanisms, and cofactor usage (2). One of the hallmarks of the NQR family is the use of riboflavin as a redox-active molecule. NQR is the only enzyme reported that directly uses this molecule as a cofactor (23, 23, 32); all other flavoenzymes use FMN or FAD. Thus, characterizing the riboflavin-binding site of NQR and its mechanisms for stabilizing catalytic intermediates is essential for a complete understanding of flavin biochemistry and biological redox mechanisms. Moreover, the uniqueness of NQR structural motifs and the lack of riboflavin in other enzymes suggest that this binding site could be a promising target for antibiotic development.

The structure of NQR obtained at low resolution (>3.5 Å), showed an electron density superficially bound to subunits B and E, directly in contact with the membrane environment, which was interpreted as riboflavin (5) (Fig. 1*B*). However, previous results show that the catalytic riboflavin-binding site is deeply buried in the structure, as this cofactor cannot be protonated (1, 23, 33) and it is resistant to strong oxidants, including oxygen (23, 33). Moreover, the "crystallographic" site is more than 30 Å away and on the opposite side in the complex from its redox partners FMN_B and UQ (26), which further indicates that this position is not the actual location of the cofactor. In this study, we propose that the riboflavin-binding site in NQR is located in a seemingly empty pocket in subunit B that contains several absolutely conserved residues, including N200, N203, and D346 (Figs. 1*C* and 3*B*). The data shown here place riboflavin within reasonable distance from its redox partners FMN_B and UQ. The results presented here offer a clear picture of the electron transfer chain by NQR. Moreover, our results allow us to characterize the only known riboflavin cofactor-binding motif involved in biochemical catalysis.

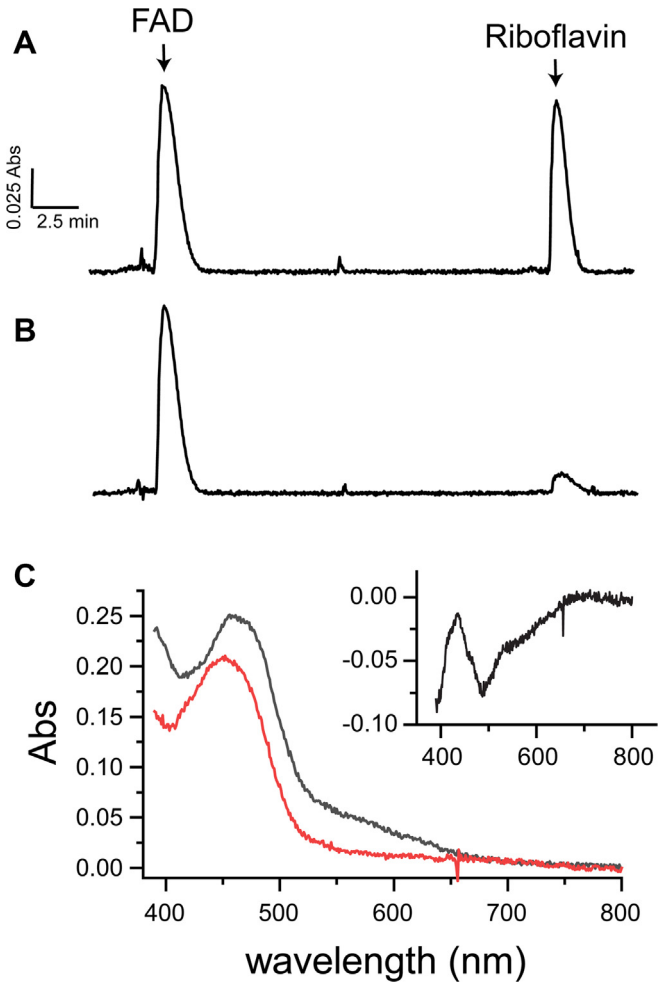

Figure 2. Riboflavin content and UV-visible spectra of WT NQR and mutants. *A*, FPLC chromatogram of noncovalently bound flavins in WT NQR (*A*) and the double mutant B-N203A/B-D346A (*B*). *C*, UV-visible spectra were measured in native conditions for WT NQR (*black line*) and the double mutant B-N203A/B-D346A. Inset: double mutant minus WT difference spectra.

Results

Mutagenesis analysis

In this work, we have identified the location of the riboflavin-binding site in a seemingly empty amphipathic pocket in subunit B (Fig. 1*C*). Empty pockets are unlikely structural components of membrane proteins, since they decrease the stability of the complex and should collapse as the protein folds. The pocket that we identified contains several absolutely conserved residues, in particular N200, N203, and D346 (Fig. 1*C*), which indicates that it likely plays a significant role in NQR structure or function. This pocket was proposed to be part of the sodium translocation channel (22), carrying residues such as D346 that were proposed to be important for sodium transport (31, 34). Alanine scanning mutagenesis was carried out on residues Asn-200, Asn203, and Asp-346, which are absolutely conserved in the family (Fig. 3*B*), initially to study their possible role in sodium translocation. To understand the participation of these residues in the catalytic mechanism of the NQR complex, the mutant enzymes were purified and characterized. NQR has three modules that can act semi-independently: NADH dehydrogenase, UQ reductase, and NADH oxidase. While the physiologic activity of NQR is the redox transfer from NADH to UQ (UQ_{RED}), it can also oxidize NADH using oxygen as electron acceptor ($NADH_{OX}$), when UQ is absent or when electron transfer is blocked. These two activities are coupled to the NADH dehydrogenase module ($NADH_{DH}$), which feeds electrons to UQ or oxygen. The three activities were measured in the mutants and WT NQR, using near-saturating concentrations of the three substrates (250 μM NADH, 50 μM UQ, and 50 mM NaCl). The UQ_{RED} activities of the three single mutants show a significant decrease, ranging from 30% to 70%, with a proportional increase in the $NADH_{OX}$ activity, while the $NADH_{DH}$ activity remains largely unmodified (Table 1). The double mutants B-N200A/B-D346A and B-N203A/B-D346A showed even lower activity of 10% to 20%. The data indicate that these mutants do not produce a general destabilization of the complex, as the $NADH_{DH}$ and $NADH_{OX}$ modules remain highly active, but a specific decrease in the electron transfer to UQ.

Enzymatic characterizations were also carried out on mutants of the riboflavin site proposed previously. In the crystallographic model, B-E402 and E-F39 appear to make hydrogen bonds and hydrophobic interactions, respectively, with the isoalloxazine ring of riboflavin (22), and their mutation should destabilize the cofactor from the site and abolish NQR activity. Interestingly, none of the residues in the crystallographic site, including B-E402 and E-F39, are conserved in the family. The mutants B-E402A and E-F39A do not produce any effect on the activity compared to the WT enzyme (Table 1). This result indicates that this site does not carry a catalytically relevant role and thus that it does not contain the riboflavin cofactor, consistent with its lack of conservation and the large distances that separate this site from riboflavin's redox partners.

Kinetic characterization of mutants

The single mutants B-N200A, B-N203A, and B-D346A, as well as the double mutants B-N200A/B-D346A and B-N203A/B-N-346A, were characterized to understand the role that these residues play in NQR mechanism. To calculate the K_m and k_{cat} kinetic constants, NADH, UQ, and NaCl titrations were carried out, maintaining the other substrates at near-saturating concentrations. As shown in Table 2, no effects were observed on the K_m for NADH, UQ, or sodium, indicating that the mutants do not modify the apparent affinity of the substrate-binding sites and also that they do not destabilize the protein structure or have long-range effects. These results show that this pocket does not have a significant role in sodium transport, in contrast with previous hypotheses (24, 31, 34). The five mutants showed a significant decrease in the k_{cat} values, suggesting that the mutations alter internal steps of the electron transfer process, which involves the cofactors, rather than sodium transport.

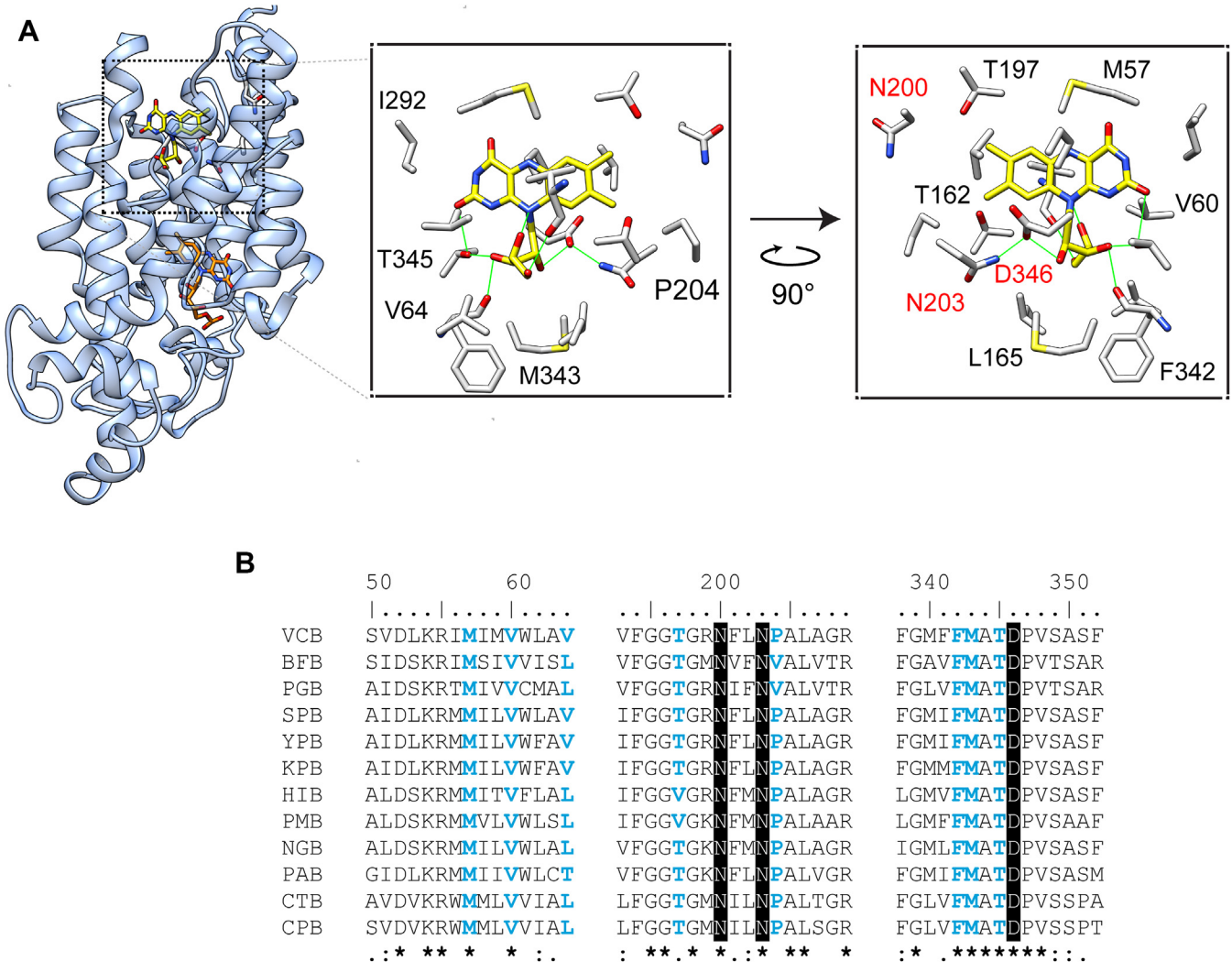

Figure 3. Location of the riboflavin-binding site. *A*, riboflavin-binding structure in subunit B. *Left panel*: Predicted pose of riboflavin (*yellow*) and FMN_B (*orange*) in the proposed pocket of subunit B (semitransparent *blue*) after MD simulation. Zoom into the riboflavin-binding position several residues that interact with riboflavin. The *center panel* shows the same orientation as the *left panel*. In the *right panel* the structure is rotated vertically by 90°. *B*, sequence alignment residues involved in riboflavin binding. The conserved residues N200, N203, and D346 are highlighted in *black* background. Residues identified in this study as part of the riboflavin site are shown in *blue*. *Bacteroides fragilis* (BF), *Chlamydia trachomatis* (CT), *Haemophilus influenza* (HI), *Klebsiella pneumoniae* (KP), *Neisseria gonorrhoeae* (NG), *Porphyromonas gingivalis* (PG), *Serratia proteomaculans* (SP), *Pseudomonas aeruginosa* (PA), *Vibrio cholerae* (VC), *Yersinia pestis* (YP). MD, molecular dynamics.

Flavin content

To understand the steps in the catalytic mechanism that are affected by the mutants, an analysis of the flavin cofactors was carried out. The total flavin content was analyzed to study possible interference of the mutations with the binding of riboflavin or other cofactors. As shown in Table 2, the individual mutants show a lower content of flavins that was not significantly different compared to the WT enzyme, which contains four flavins: FAD, riboflavin, and two FMN molecules. Interestingly, the two double mutants show a flavin:-protein ratio of nearly three, indicating that one of the flavins is lost due to the mutations. To pinpoint the flavin that is lost in the double mutants, SDS-PAGE analysis was carried out. In all single and double mutants, two fluorescent bands were observed in SDS-PAGE gels exposed to UV light (not shown). These bands correspond to the covalently attached FMN to subunits B and C (35), indicating that the mutations do not interfere with FMN incorporation to the complex. Analysis of the noncovalently bound flavins FAD and riboflavin was carried out by reverse-phase HPLC in WT NQR and the double

Table 1
Activities of NQR mutants

Mutant	Turnover rate (s^{-1})		
	$NADH_{DH}$	UQ_{RED}	$NADH_{OX}$
Wild -type	530 ± 25	505 ± 33	41 ±11
B-N200A	455 ± 33	352 ± 44[a]	70 ± 7[a]
B-N203A	489 ± 56	218 ± 5[a]	260 ± 10[a]
B-D346A	477 ± 51	156 ± 32[a]	310 ± 29[a]
B-N200A/B-D346A	505 ± 50	107 ± 12[a]	381 ± 11[a]
B-N203A/B-D346A	503 ± 45	58 ± 10[a]	447 ± 27[a]
B-E402A	497 ± 46	488 ± 22	62 ± 22
E-F39A	483 ± 13	468 ± 42	28 ± 10

The activities were measured at a fixed concentration of the three substrates (250 μM NADH, 50 mM NaCl, and 50 μM UQ).
[a] $p < 0.05$ *versus* WT activity (n > 4).

Table 2
Kinetic parameters of mutant and WT NQR

Mutant	k_{cat} (s^{-1})	Km_{app} NADH (μM)	Km_{app} UQ-1 (μM)	Km_{app} NaCl (mM)	Flavin: Protein	Riboflavin: FAD
WT	550 ± 25	25 ± 10	2.9 ± 0.5	3.5 ± 1.1	3.7 ± 0.2	0.8
B-N200A	350 ± 25[a]	27 ± 4	3 ± 0.6	4.2 ± 1.8	3.5 ± 0.3	
B-N203A	235 ± 21[a]	33 ± 3	3 ± 0.6	3.7 ± 1.8	3.4 ± 0.3	
B-D346A	155 ± 34[a]	33 ± 4	2.8 ± 0.5	3.3 ± 1.5	3.3 ± 0.3	
B-N200A/B-D346A	115 ± 29[a]	31 ± 3	2.5 ± 1.5	2.6 ± 0.9	2.9 ± 0.1[a]	<0.1
B-N203A/B-D346A	64 ± 5[a]	24 ± 2	2.4 ± 1	3 ± 0.9	2.7 ± 0.1[a]	<0.05

The reported k_{cat} corresponds to the physiologic UQ_{RED} activity of the enzyme. k_{cat} and Km_{app} values were calculated by fitting the saturation curves to the Michaelis–Menten equation. Activities were measured at different concentrations of one substrate at constant and near-saturating concentrations of the other two substrates.
[a] $p < 0.05$ *versus* WT activity (n > 4).

mutants. As shown in Figure 2, riboflavin is almost completely absent in the double mutant B-N203A/B-D346A (Fig. 2*B*), in contrast with WT NQR, in which it has a 1:1 ratio compared to FAD (Fig. 2*A* and Table 2).

Riboflavin cofactor reduction state

To further characterize the effects of the mutants on the properties of riboflavin as a cofactor, the stability and presence of the riboflavin neutral radical, a hallmark of the NQR family, were examined. In the air-oxidized state of NQR, riboflavin is found as a neutral semiquinone radical (23, 33), which can be characterized by UV-visible spectroscopic methods. Figure 2*C* shows the spectra of WT NQR and the double mutant B-N203A/B-D346A. As can be observed, the double mutant lacks the absorption shoulder from 500 to 700 nm, attributed to the riboflavin neutral radical (17, 23). The difference spectrum of the double mutant minus WT NQR shows the characteristic absorption of the riboflavin neutral radical (Fig. 2*C*, Inset), with minima at 490 nm and shoulders from 500 to 700 nm (23). Altogether, the data indicate that the residues in the hydrophobic pocket play an important role in the binding of riboflavin to NQR.

Molecular modeling

Calculations were carried out to generate an atomistic model of the riboflavin-binding site. Molecular docking of riboflavin to the crystallographic structure yielded a binding pose with an AutoDock Vina score of −6 kcal/mol (Fig. S1), indicating that the site has suitable properties to bind this cofactor. However, it is possible that riboflavin sits deeper in the site or adopts a different pose, as the structure was not obtained under physiologic conditions (high salt concentration and high pH (22)). Therefore, we decided to carry out molecular dynamics (MD) simulations to better understand the riboflavin-binding site. In the model, NQR is incorporated into a membrane bilayer in a medium that includes explicit water molecules and ions. Three independent MD simulations were performed to relax the structure and to evaluate the stability of riboflavin in the proposed site (Fig. S2). As a comparison, we also performed three independent simulations of riboflavin in the crystallographic site. In all the simulations, whether riboflavin was placed in the crystallographic or proposed sites, the structure of the protein stabilized with a RMSD of alpha carbons of around 4.5 Å from the initial model (Fig. S2). On the other hand, the behavior of riboflavin markedly differed between the two sets of simulations. For simulations in the proposed site, the isoalloxazine ring of riboflavin rotated within the pocket. In two of the three simulations, the RMSD stabilized at less than 4 Å from the initial model. In the third, the RMSD is less than 6 Å. In all three simulations, riboflavin remained within the pocket and established similar contacts with the NQR structure (Fig. S3). In contrast, riboflavin was much less stable in the crystallographic site, moving by more than 5 Å as soon as restraints were released. In one of the three simulations, the molecule completely dissociated from the binding pocket. In the final snapshot of the trajectories, AutoDock Vina scores for riboflavin binding to NQR were −2.7 (for the dissociated riboflavin), −3.7, and −3.6 kcal/mol for the crystallographic site and −8.5, −9.5, and −10 kcal/mol for the proposed site. These results indicate that riboflavin can fit into and form much stronger interactions with the proposed site than with the crystallographic site. Indeed, riboflavin establishes favorable interactions with several residues in the pocket, including hydrogen bonds with the peptide backbone of residues F342 and V161, and the side chains of residues T345, as well as the mutated residues D346 and N203, which significantly decrease the activity of the enzyme. As shown in Figure 3*B*, these residues are conserved in the family, supporting the biochemical and computational data.

Discussion

Location and structure of the catalytic riboflavin-binding site

The NQR crystal structure obtained at relatively low resolution (>3.5 Å) shows the presence of an electron density that was interpreted as riboflavin (22). The crystallographic riboflavin is superficially bound to the interface of subunits B and E (Fig. 1*B*). However, this location is highly problematic, as this site is too far away (>30 Å) from riboflavin's redox partners, FMN_B and UQ. Moreover, this location does not have any conserved residues and does not have the expected properties of the riboflavin-binding site, such as a deeply buried location shielded from protons and oxidants (22). As shown in this report, the mutations to B-E402 and E-F39, which are part of the crystallographic site, do not produce significant effects on the activity. Moreover, our MD simulations shown that the binding of riboflavin to this site is weak and the molecule can be easily dissociated. The data indicate that the crystallographic site does not carry the catalytic riboflavin cofactor.

Identification of NQR's riboflavin-binding site

In this report, we propose a novel site that appears as an empty amphipathic pocket in the published tridimensional structure. This pocket was previously suggested as the entry vestibule for sodium (22), as it contains residues that were identified as essential for sodium translocation, including D-346 (31, 34). However, a close examination of the pocket reveals that it does not have the typical architecture of entry channels observed in other pumps, being tooth shaped, too wide for sodium, and with several cavities (Fig. 1, *B* and *C*), rather than a relatively narrow passageway lined with negatively charged or polar residues to guide sodium through the membrane. Moreover, the pocket is directly on top of FMN_B and there are no evident exit pathways for sodium. As shown in this report, the single and double mutants of three absolutely conserved residues found in this pocket, B-N200, B-N203 and B-D346, do not affect the K_m for sodium or any other substrate, strongly suggesting that the pocket is not involved in sodium transport.

While the mutations do not produce any effects on the K_m for the substrates, a decrease in the UQ_{RED} activity was found, indicating that electron transfer is impaired in the mutants. Examination of the flavin content show that double mutants B-N200/B-D346 and B-N203/B-D346 specifically lack riboflavin, as well as the neutral semiquinone radical signal associated with this cofactor. Docking analysis shows that the pocket can accommodate riboflavin (Fig. S1), further supporting the hypothesis that this is the riboflavin-binding site. MD simulations offer a better picture of the way in which the cofactor is bound to the site. Residues N203 and D346 appear to make hydrogen bonds with riboflavin, explaining the observed behavior of the mutants. The MD data show that riboflavin establishes hydrogen bonds with many residues, and thus, it is not expected that the elimination of one residue by site-directed mutagenesis would prevent the binding of the cofactor to the site, which may explain the need to eliminate two residues in the double mutant. Interestingly, residue N200 does not appear to make contacts with riboflavin, although the mutants of this residue reduce the activity of the enzyme. One possibility is that N200 is structurally important to the site, but it should also be considered that the MD simulation does not completely recapitulate the native form of NQR. Further experiments will be required to address this issue.

The riboflavin-binding sites of other proteins such as the ABC-type riboflavin transporter, riboflavin-binding protein, the riboflavin-binding immunoglobulin IgG^{GAR}, and riboflavin kinase are also rich in polar or charged residues, including serine, glutamate, aspartate, and lysine, which interact with the ribityl moiety of riboflavin (36–39). In contrast with these sites, which are readily accessible to the aqueous environment and can quickly exchange riboflavin and the reaction products of these enzymes and proteins (*i.e.*, FAD and FMN), riboflavin goes more deeply in the proposed pocket (Fig. 3*A*), which is capped by subunit A that sits on top, consistent with the pH titration data, showing that the riboflavin cofactor is unable to exchange protons with the aqueous environment (40). Moreover, a buried site is also consistent with the environment required to shield the riboflavin neutral radical from oxygen and other strong oxidants (23, 32, 41). Altogether, the evidence strongly supports that this is the elusive NQR riboflavin-binding site.

Electron transfer chain

The location of the riboflavin-binding site described here provides a definitive answer to understand the way in which the electrons are transferred though NQR. Previous reports indicate that the redox equivalents follow the next pathway: NADH → FAD → 2Fe-2S → FMN_C → FMN_B → riboflavin → UQ (26, 31). This pathway has been corroborated through the study of the redox properties of the cofactors, showing that the redox potential increases stepwise along the pathway (31). While the crystallographic data provide important structural information, it is incomplete and has yet to be fully reconciled with biochemical data. The data show that the 2Fe-2S center and FMN_C are located on opposite sides of the membrane and that they are probably connected through the novel nonheme iron center, located in membrane subunits D and E (22). However, experimental evidence regarding its participation in electron transfer is still missing. Other aspects that were unclear from the crystal structure were the binding sites of NADH and UQ, which were not observed in the electron density. Finally, as we have already discussed, there is only weak evidence for the crystallographic binding site of riboflavin.

The riboflavin-binding site that we have identified lies at a shorter distance (20 Å) between FMN_B and the predicted UQ-binding site (Fig. 4), compared to the crystal structure. Analysis of the stopped flow data previously reported (23, 26, 31) indicate that the rate of electron transfer of the lower part of the internal electron transfer chain, FMN_B → riboflavin → UQ, is $> 2000\ s^{-1}$, strongly indicating that these three cofactors lie in close contact. It should be noted that the crystal structure reported might not represent conformation of NQR under physiologic conditions, and some of these distances could actually be smaller, in particular if riboflavin gets deeper into the pocket. Other groups have proposed that the UQ-binding site is located in the hydrophilic subunit A (24, 25) and that the electron transfer chain might involve the crystallographic riboflavin site. However, as shown in this report, mutations in the crystallographic riboflavin site do not produce any changes in the activity of the enzyme. Moreover, this site does not have the properties expected for a functional site and it is too far away from both FMN_B and either of the two UQ sites. Some groups have proposed a convoluted mechanism in which conformational changes could allow a close interaction of subunit A with the crystallographic riboflavin site (25). However, large conformational changes are not consistent with the high electron transfer rate of the lower part of the internal electron transfer chain. Moreover, these changes only take into account the position of riboflavin and UQ and cannot account for the large distance that separates FMN_B and riboflavin (>30 Å). Finally, this hypothesis has serious thermodynamic complications as the transfer of electrons from riboflavin to UQ releases less than 9 kJ/mol (42), a modest amount of

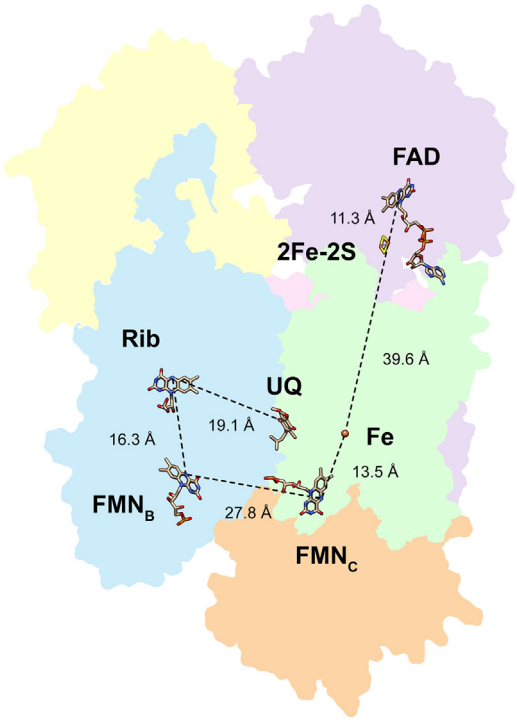

Figure 4. Distance between riboflavin and other cofactors in NQR. The figure shows the locations of subunits A (*yellow*), B (*blue*), C (*orange*), D (*green*), E (*pink*), and F (*violet*) and the locations and distances between cofactors.

energy to drive a conformational change of this magnitude, which is not even related to sodium translocation and thus appears to be superfluous.

In a previous publication, we discussed that the location of the UQ site in the cytosolic subunit A is highly unlikely, due to the lack of conservation of the presumptive site and the need for the highly hydrophobic ubiquinone molecule to be pulled out of the membrane to interact in the hydrophilic site (33), a mechanism not seen or proposed for any respiratory enzyme. Moreover, the location of the site in subunit A is based primarily on the labeling with UQ analogs (24, 43, 44), which are notorious for their unspecific labeling, and in fact in NQR they seem to label mostly hydrophilic lysine residues. In contrast, the location proposed by our group in the interface of subunits B and D (Fig. 1, *A* and *B*) is much more likely, as it is found in a fully conserved site located in the membrane bilayer, with easy access to the benzoquinone head of UQ (13). Moreover, we have shown that mutations in this site confer resistance to the natural UQ analog HQNO, allowing *P. aeruginosa* to survive autopoisoning (17). Moreover, this site is in close proximity to residues B-G141 and B-G140, which have shown to confer resistance to the UQ analog korormycin (45). Crystallographic data with brominated ubiquinone analogs show UQ in the position that was predicted by our group (33). Altogether, the location of the riboflavin site that we are proposing in this work and the UQ site that we described previously offer a parsimonious and economical mechanism to explain electron transfer in the NQR complex.

Conclusion

The results presented here allow us to propose, for the first time, the structure of the riboflavin-binding site for the only enzyme known to use this molecule as a cofactor. Moreover, our results provide a clear pathway to understand electron transfer in NQR, an essential bacterial respiratory complex.

Experimental procedures

Site-directed mutagenesis

To identify and map the riboflavin-binding site, *V. cholerae* NQR mutants were obtained using QuikChange site-directed mutagenesis kits. The selected residues were mutated to alanine using the *V. cholerae* nqr pBAD/HisB construct as previously described (33). The primers used in this study are listed in Table 3.

Protein purification

V. cholerae Δnqr cells carrying the WT or mutant NQR pBAD/HisB plasmids were cultured in LB media, as described before (34). Expression of NQR mutants was induced with 0.05% (w/v) arabinose. Induced cells were harvested at the early stationary phase by centrifugation at 4000 rpm. The cells were resuspended in buffer containing 50 ng/ml DNAase-I, 5 mM $MgCl_2$, 1 mM PMSF, 50 mM Na_2HPO_4, 5 mM imidazole, and 300 mM NaCl, pH 8.0. Cells were lysed in a high-pressure homogenizer (Avestin Emulsiflex C5) at 16,000 psi. Cell debris was removed by differential centrifugation, and the cell membranes were collected by centrifugation at 67,000*g* for 3 h (46). The membranes were solubilized in buffer containing 0.3% n-dodecyl-β-D-maltoside (DDM), 5 mM imidazole, 50 mM Na_2HPO_4, 300 mM NaCl, and 5% glycerol, pH 8.0. NQR was purified following two chromatographic steps, nickel-nitrilotriacetic acid affinity chromatography and diethylaminoethanol-Sepharose ion-exchange chromatography, as described before (27), obtaining a purity >93% for all mutants based on the densitometric proportion of the bands obtained after SDS-PAGE.

Activity measurements

To investigate the properties of the mutants, steady-state kinetic experiments were performed in buffer containing 50 mM Tris, 50 mM NaCl, 5% glycerol, and 0.05% DDM, pH 8.0, as described previously (13). NADH dehydrogenase and UQ reductase activity were measured spectrophotometrically at 340 nm (ε_{NADH} = 6.22 mM^{-1} cm^{-1}) and 282 nm ($\varepsilon_{UQ\text{-}UQH2}$ = 11.8 mM^{-1} cm^{-1}) (34). NADH oxidase activity

Table 3
Primers used in this study

Mutation	Sequence of forward primer (5′ – 3′)
B-N200A	GGTGGTACAGGCCGTGCCTTCCTTAACCCAGC
B-N203A	GCCGTAACTTCCTTGCCCCAGCGCTGGCTG
B-D346A	TCTTCATGGCGACTGCCCCAGTTTCTGCGTC
B-E402A	TTGACCATGTGGTTGTAGCGAGAAATATCAAGCGGAG
E-F39A	TCGAAGAAAGTTAAGACATCAGCCGGCTTAGGTATTG CGGTAATC

was measured as the difference between NADH dehydrogenase and UQ reductase activity. Activity kinetic measurements of each mutant were conducted in the presence of varying concentrations of the substrate UQ (0–30 μM), NADH (0–250 μM), or NaCl (0–50 mM) (33).

Spectral analysis

The UV-visible absorption spectra of WT and mutant NQR were analyzed spectrophotometrically. The absorption spectra of the samples were measured under native conditions in buffer containing 50 mM Tris, 50 mM NaCl, 5% glycerol, and 0.05% DDM, pH 8.0.

Flavin content analysis

Flavin content was measured spectrophotometrically at 450 nm in the purified samples and was compared with the protein concentration, measured through the bicinchoninic acid assay (47), to obtain flavin:protein ratios. The content of noncovalently attached FAD and riboflavin was measured using HPLC chromatography, as described before (23, 48). Briefly, 100 μM of WT and mutants were denatured in 2% SDS to a final volume of 500 μl. The denatured samples were filtered through a 10 kDa Amicon concentrator. The filtrate was collected and analyzed by reverse-phase HPLC, using a 100-5-C18 column and using 5 mM ammonium acetate:methanol (80:20) as the mobile phase (23).

Molecular modeling

NQR was modeled in a similar way to Willow *et. al* (49). A key difference is that we performed simulations in which riboflavin was docked into our newly proposed site in addition to simulations where it is in the crystallographic pose. Starting with the homology model of the complex, riboflavin was docked into the proposed site using AutoDock Vina 1.1.2 (50). Based on the SMILES string from the ZINC database (51) (accession number ZINC2036848), the structure of riboflavin was built and minimized using UCSF Chimera 1.14 (52). Polar hydrogens and Gasteiger charges were added to the homology model using Dock Prep in Chimera. Molecular docking was performed using AutoDock Vina with a docking grid of 22 ×14 × 22 Å located in our proposed site in subunit B. In order to collect many possible binding modes, exhaustiveness was set to 8 individual runs in parallel and a maximum energy range of 3 was selected.

For the MD simulations, we used the same force field and initial structure of the protein as in Willow *et. al* (49). The main differences between simulations in the present and previous study are in the placement of riboflavin, determination of protonation states, length of simulation, and number of repetitions. Whereas in the previous study we used AMBER default protonation states, here we calculated energetically favorable amino acid protonation states using PDB2PQR 3.1.0 (53). In the previous study, we performed one simulation with 20 ns of equilibration and 80 ns of production. Here, we performed six total simulations, each with 6 ns of equilibration and 10 ns of production. In both studies, the equilibration process was based on python codes provided in the Membrane Builder of CHARMM-GUI (54), using more simulation time than recommended in the original code. Here, we used (1) 125 ps based on 1 fs time steps for the crystallographic site or 250 ps based on 2 fs time steps for the proposed site of canonical ensemble with constraints, (2) 125 ps of canonical ensemble without constraints, (3) 2.5 ns of NPT with MonteCarloMembraneBarostat, and (4) 2.5 ns of NPT with MonteCarloBarostat. Production runs were based on 10 ns of NPT with MonteCarloBarostat. Finally, three simulations were performed with riboflavin in the crystallographic site and three with riboflavin in the proposed site.

Data availability

The data published in this article would be available upon request to the corresponding author.

Supporting information—This article contains supporting information.

Author contributions—O. J., K. T., D. D. L. M., and J. R. F. conceptualization; O. J. and K. T. methodology; D. D. L. M., J. A. D.-B., T. T. T. D., and S. Y. W. software; O. J., K. T., and D. D. L. M. validation; O. J., K. T., and D. D. L. M. formal analysis; K. T., Y. H., M. Y., T. T. T. D., and J. A. D.-B. investigation; O. J. resources; O. J., K. T., and D. D. L. M. data curation; O. J. and K. T. writing–original draft; O. J., K. T., Y. H., M. Y., T. T. T. D., J. A.D.-B., D. D. L. M., and J. R. F. writing–review & editing; K. T., M. Y., T. T. T. D., and J. A. D.-B. visualization; O. J., D. D. L. M., and K. T. supervision; O. J. project administration; O. J. funding acquisition.

Funding and additional information—This research was supported by the National Institutes of Health: R15GM131292 (O. J.), R01GM127712 (D. D. L. M.). The content is solely the responsibility of the authors and does not necessarily represent the official views of the National Institutes of Health.

Conflict of interest—The authors declare that they have no conflicts of interest with the contents of this article.

Abbreviations—The abbreviations used are: DDM, n-dodecyl-β-D-maltoside; MD, molecular dynamics; UQ, ubiquinone.

References

1. Juárez, O., and Barquera, B. (2012) Insights into the mechanism of electron transfer and sodium translocation of the Na+-pumping NADH: quinone oxidoreductase. *Biochim. Biophys. Acta (Bba) - Bioenerg.* **1817**, 1823–1832
2. Reyes-Prieto, A., Barquera, B., and Juárez, O. (2014) Origin and evolution of the sodium -pumping NADH: ubiquinone oxidoreductase. *PLoS One*. https://doi.org/10.1371/journal.pone.0096696
3. Häse, C. C., and Barquera, B. (2001) Role of sodium bioenergetics in Vibrio cholerae. *Biochim. Biophys. Acta* **1505**, 169–178
4. Bogachev, A. V., and Verkhovsky, M. I. (2005) Na(+)-Translocating NADH:quinone oxidoreductase: progress achieved and prospects of investigations. *Biochem. Mosc* **70**, 143–149
5. Steuber, J., Vohl, G., Muras, V., Toulouse, C., Claußen, B., Vorburger, T., *et al.* (2015) The structure of Na^+-translocating of NADH:ubiquinone

oxidoreductase of Vibrio cholerae: implications on coupling between electron transfer and Na^+ transport. *Biol. Chem.* **396**, 1015–1030
6. Verkhovsky, M. I., and Bogachev, A. V. (2010) Sodium-translocating NADH:quinone oxidoreductase as a redox-driven ion pump. *Biochim. Biophys. Acta (Bba) - Bioenerg.* **1797**, 738–746
7. Vorburger, T., Nedielkov, R., Brosig, A., Bok, E., Schunke, E., Steffen, W., *et al.* (2016) Role of the Na+-translocating NADH:quinone oxidoreductase in voltage generation and Na+ extrusion in Vibrio cholerae. *Biochim. Biophys. Acta (Bba) - Bioenerg.* **1857**, 473–482
8. Dibrov, P., Dibrov, E., and Pierce, G. N. (2017) Na+-NQR (Na+-translocating NADH:ubiquinone oxidoreductase) as a novel target for antibiotics. *FEMS Microbiol. Rev.* **41**, 653–671
9. Kojima, S., Yamamoto, K., Kawagishi, I., and Homma, M. (1999) The polar flagellar motor of Vibrio cholerae is driven by an Na+ motive force. *J. Bacteriol.* **181**, 1927–1930
10. Häse, C. C., Fedorova, N. D., Galperin, M. Y., and Dibrov, P. A. (2001) Sodium ion cycle in bacterial pathogens: evidence from cross-genome comparisons. *Microbiol. Mol. Biol. Rev.* **65**, 353–370
11. Häse, C. C., and Mekalanos, J. J. (1999) Effects of changes in membrane sodium flux on virulence gene expression in Vibrio cholerae. *PNAS* **96**, 3183–3187
12. Häse, C. C., and Mekalanos, J. J. (1998) TcpP protein is a positive regulator of virulence gene expression in Vibrio cholerae. *Proc. Natl. Acad. Sci. U. S. A.* **95**, 730–734
13. Raba, D. A., Yuan, M., Fang, X., Menzer, W. M., Xie, B., Liang, P., *et al.* (2019) Role of subunit D in ubiquinone-binding site of Vibrio cholerae NQR: pocket flexibility and inhibitor resistance. *ACS Omega* **4**, 19324–19331
14. Liang, P., Rosas-Lemus, M., Patel, D., Fang, X., Tuz, K., and Juárez, O. (2018) Dynamic energy dependency of Chlamydia trachomatis on host cell metabolism during intracellular growth: role of sodium-based energetics in chlamydial ATP generation. *J. Biol. Chem.* **293**, 510–522
15. Malhotra, M., Sood, S., Mukherjee, A., Muralidhar, S., and Bala, M. (2013) Genital Chlamydia trachomatis: an update. *Indian J. Med. Res.* **138**, 303–316
16. O'Connell, C. M., and Ferone, M. E. Chlamydia trachomatis genital infections. Microb. Cell. 3, 390–403
17. Raba, D. A., Rosas-Lemus, M., Menzer, W. M., Li, C., Fang, X., Liang, P., *et al.* (2018) Characterization of the Pseudomonas aeruginosa NQR complex, a bacterial proton pump with roles in autopoisoning resistance. *J. Biol. Chem.* **293**, 15664–15677
18. Fazeli, H., Akbari, R., Moghim, S., Narimani, T., Arabestani, M. R., and Ghoddousi, A. R. (2012) Pseudomonas aeruginosa infections in patients, hospital means, and personnel's specimens. *J. Res. Med. Sci.* **17**, 332–337
19. Hirsch, E. B., and Tam, V. H. (2010) Impact of multidrug-resistant Pseudomonas aeruginosa infection on patient outcomes. *Expert Rev. Pharmacoecon Outcomes Res.* **10**, 441–451
20. Aloush, V., Navon-Venezia, S., Seigman-Igra, Y., Cabili, S., and Carmeli, Y. (2006) Multidrug-resistant Pseudomonas aeruginosa: risk factors and clinical impact. *Antimicrob. Agents Chemother.* **50**, 43–48
21. Dibrov, P., Dibrov, E., Maddaford, T. G., Kenneth, M., Nelson, J., Resch, C., *et al.* (2017) Development of a novel rationally designed antibiotic to inhibit a nontraditional bacterial target. *Can. J. Physiol. Pharmacol.* **95**, 595–603
22. Steuber, J., Vohl, G., Casutt, M. S., Vorburger, T., Diederichs, K., and Fritz, G. (2014) Structure of the V. cholerae Na + -pumping NADH: quinone oxidoreductase. *Nature* **516**, 62–67
23. Juárez, O., Nilges, M. J., Gillespie, P., Cotton, J., and Barquera, B. (2008) Riboflavin is an active redox cofactor in the Na+-pumping NADH: quinone oxidoreductase (Na+-NQR) from Vibrio cholerae. *J. Biol. Chem.* **283**, 33162–33167
24. Casutt, M. S., Nedielkov, R., Wendelspiess, S., Vossler, S., Gerken, U., Murai, M., *et al.* (2011) Localization of ubiquinone-8 in the Na+-pumping NADH:quinone oxidoreductase from Vibrio cholerae. *J. Biol. Chem.* **286**, 40075–40082
25. Ito, T., Murai, M., Ninokura, S., Kitazumi, Y., Mezic, K. G., Cress, B. F., *et al.* (2017) Identification of the binding sites for ubiquinone and inhibitors in the Na+-pumping NADH-ubiquinone oxidoreductase from Vibrio cholerae by photoaffinity labeling. *J. Biol. Chem.* **292**, 7727–7742
26. Juárez, O., Morgan, J. E., and Barquera, B. (2009) The electron transfer pathway of the Na+-pumping NADH:quinone oxidoreductase from Vibrio cholerae. *J. Biol. Chem.* **284**, 8963–8972
27. Tuz, K., Mezic, K. G., Xu, T., Barquera, B., and Juárez, O. (2015) The kinetic reaction mechanism of the Vibrio cholerae sodium-dependent NADH dehydrogenase. *J. Biol. Chem.* **290**, 20009–20021
28. Bertsova, Y. V., Fadeeva, M. S., Kostyrko, V. A., Serebryakova, M. V., Baykov, A. A., and Bogachev, A. V. (2013) Alternative pyrimidine biosynthesis protein ApbE is a flavin transferase catalyzing covalent attachment of FMN to a threonine residue in bacterial flavoproteins. *J. Biol. Chem.* **288**, 14276–14286
29. Fang, X., Osipiuk, J., Chakravarthy, S., Yuan, M., Menzer, W. M., Nissen, D., *et al.* (2019) Conserved residue His-257 of Vibrio cholerae flavin transferase ApbE plays a critical role in substrate binding and catalysis. *J. Biol. Chem.* **294**, 13800–13810
30. Belevich, N. P., Bertsova, Y. V., Verkhovskaya, M. L., Baykov, A. A., and Bogachev, A. V. (2016) Identification of the coupling step in Na+-translocating NADH:quinone oxidoreductase from real-time kinetics of electron transfer. *Biochim. Biophys. Acta (Bba) - Bioenerg.* **1857**, 141–149
31. Juárez, O., Morgan, J. E., Nilges, M. J., and Barquera, B. (2010) Energy transducing redox steps of the Na+-pumping NADH:quinone oxidoreductase from Vibrio cholerae. *PNAS* **107**, 12505–12510
32. Barquera, B., Zhou, W., Morgan, J. E., and Gennis, R. B. (2002) Riboflavin is a component of the Na+-pumping NADH-quinone oxidoreductase from Vibrio cholerae. *Proc. Natl. Acad. Sci. U.S.A.* **99**, 10322–10324
33. Tuz, K., Li, C., Fang, X., Raba, D. A., Liang, P., Minh, D. D. L., *et al.* (2017) Identification of the catalytic ubiquinone-binding site of Vibrio cholerae sodium-dependent NADH dehydrogenase. *J. Biol. Chem.* **292**, 3039–3048
34. Juárez, O., Athearn, K., Gillespie, P., and Barquera, B. (2009) Acid residues in the transmembrane helices of the Na+-pumping NADH:quinone oxidoreductase from Vibrio cholerae involved in sodium translocation. *Biochemistry* **48**, 9516–9524
35. Barquera, B., Häse, C. C., and Gennis, R. B. (2001) Expression and mutagenesis of the NqrC subunit of the NQR respiratory Na(+) pump from Vibrio cholerae with covalently attached FMN. *FEBS Lett.* **492**, 45–49
36. Deka, R. K., Brautigam, C. A., Biddy, B. A., Liu, W. Z., and Norgard, M. V. (2013) Evidence for an ABC-type riboflavin transporter system in pathogenic spirochetes. *mBio* **4**, e00615-12
37. Duurkens, R. H., Tol, M. B., Geertsma, E. R., Permentier, H. P., and Slotboom, D. J. (2007) Flavin binding to the high affinity riboflavin transporter RibU. *J. Biol. Chem.* **282**, 10380–10386
38. Zhu, X., Wentworth, P., Kyle, R. A., Lerner, R. A., and Wilson, I. A. (2006) Cofactor-containing antibodies: crystal structure of the original yellow antibody. *Proc. Natl. Acad. Sci. U. S. A.* **103**, 3581–3585
39. Karthikeyan, S., Zhou, Q., Mseeh, F., Grishin, N. V., Osterman, A. L., and Zhang, H. (2003) Crystal structure of human riboflavin kinase reveals a β barrel fold and a novel active site. *Arch.* Struct. **11**, 265–273
40. Toulouse, C., Claussen, B., Muras, V., Fritz, G., and Steuber, J. (2017) Strong pH dependence of coupling efficiency of the Na+ – translocating NADH:quinone oxidoreductase (Na+-NQR) of Vibrio cholerae. *Biol. Chem.* **398**, 251–260
41. Barquera, B., Morgan, J. E., Lukoyanov, D., Scholes, C. P., Gennis, R. B., and Nilges, M. J. (2003) X- and W-band EPR and Q-band ENDOR studies of the flavin radical in the Na+-Translocating NADH:quinone oxidoreductase from Vibrio cholerae. *J. Am. Chem. Soc.* **125**, 265–275
42. Neehaul, Y., Juárez, O., Barquera, B., and Hellwig, P. (2012) Thermodynamic contribution to the regulation of electron transfer in the Na+-Pumping NADH:quinone oxidoreductase from Vibrio cholerae. *Biochemistry* **51**, 4072–4077
43. Strickland, M., Juárez, O., Neehaul, Y., Cook, D. A., Barquera, B., and Hellwig, P. (2014) The conformational changes induced by ubiquinone binding in the Na+-pumping NADH:ubiquinone oxidoreductase (Na+-NQR) are kinetically controlled by conserved glycines 140 and 141 of the NqrB subunit. *J. Biol. Chem.* **289**, 23723–23733

44. Nedielkov, R., Steffen, W., Steuber, J., and Möller, H. M. (2013) NMR reveals double occupancy of quinone-type ligands in the catalytic quinone binding site of the Na+-translocating NADH:quinone oxidoreductase from Vibrio cholerae. *J. Biol. Chem.* **288**, 30597–30606
45. Yoshikawa, K., Adachi, K., Nishida, F., and Mochida, K. (2003) Planar structure and antibacterial activity of korormicin derivatives isolated from Pseudoalteromonas sp. F-420. *J. Antibiot. (Tokyo)* **56**, 866–870
46. Liang, P., Fang, X., Hu, Y., Yuan, M., Raba, D. A., Ding, J., *et al.* (2020) The aerobic respiratory chain of Pseudomonas aeruginosa cultured in artificial urine media: role of NQR and terminal oxidases. *PLoS One*. https://doi.org/10.1371/journal.pone.0231965
47. Barquera, B., Nilges, M. J., Morgan, J. E., Ramirez-Silva, L., Zhou, W., and Gennis, R. B. (2004) Mutagenesis study of the 2Fe-2S center and the FAD binding site of the Na+-translocating NADH:ubiquinone oxidoreductase from Vibrio cholerae. *Biochemistry* **43**, 12322–12330
48. Light, D. R., Walsh, C., and Marletta, M. A. (1980) Analytical and preparative high-performance liquid chromatography separation of flavin and flavin analog coenzymes. *Anal. Biochem.* **109**, 87–93
49. Willow, S. Y., Yuan, M., Juárez, O., and Minh, D. D. L. (2021) Electrostatics and water occlusion regulate covalently-bound flavin mononucleotide cofactors of Vibrio cholerae respiratory complex NQR. *Proteins* **89**, 1376–1385
50. Trott, O., and Olson, A. J. (2010) AutoDock Vina: improving the speed and accuracy of docking with a new scoring function, efficient optimization and multithreading. *J. Comput. Chem.* **31**, 455–461
51. Sterling, T., and Irwin, J. J. (2015) Zinc 15 - ligand discovery for everyone. *J. Chem. Inf. Model.* **55**, 2324–2337
52. Pettersen, E. F., Goddard, T. D., Huang, C. C., Couch, G. S., Greenblatt, D. M., Meng, E. C., *et al.* (2004) UCSF Chimera—a visualization system for exploratory research and analysis. *J. Comput. Chem.* **25**, 1605–1612
53. Jurrus, E., Engel, D., Star, K., Monson, K., Brandi, J., Felberg, L. E., *et al.* (2018) Improvements to the APBS biomolecular solvation software suite. *Protein Sci.* **27**, 112–128
54. Jo, S., Jiang, W., Lee, H. S., Roux, B., and Im, W. (2012) CHARMM-GUI ligand binder for absolute binding free energy calculations and its application. *J. Chem. Inf. Model.* **53**, 267–277